Changes in precipitation regimes over North America during the Holocene as recorded by mineralogy and geochemistry of Gulf of Mexico sediments

Jean Carlos Montero-Serrano, Viviane Bout-roumazeilles, Thomas Sionneau, Nicolas Tribovillard, Aloys Bory, Benjamin P Flower, Armelle Riboulleau, Philippe Martinez, Isabelle Billy

Changes in precipitation regimes over North America during the Holocene as recorded by mineralogy and geochemistry of Gulf of Mexico sediments

Jean Carlos Montero-Serrano [a,*], Viviane Bout-Roumazeilles [a], Thomas Sionneau [a,b], Nicolas Tribovillard [a], Aloys Bory [a], Benjamin P. Flower [c], Armelle Riboulleau [a], Philippe Martinez [d], Isabelle Billy [d]

[a] Université Lille 1, Laboratoire Géosystèmes, FRE 3298 CNRS, bâtiment SN5, 59655 Villeneuve d'Ascq cedex, France

[b] Institut Universitaire Européen de la Mer, UMR 6538 CNRS, Domaines Océaniques, Place Nicolas Copernic, 29280 Plouzané, France

[c] College of Marine Science, University of South Florida, 140 7th Avenue South, St. Petersburg, FL 33701, USA

[d] Université Bordeaux 1, EPOC, UMR - CNRS 5805, Avenue des Facultés, 33405 Talence Cedex, France

* Corresponding author. Tel.: +33 169823537; fax: +33 169823568.

E-mail addresses: jeanmontero@yahoo.es (J.C. Montero-Serrano), viviane.bout@univ-lille1.fr (V. Bout-Roumazeilles), thomas.sionneau@univ-brest.fr (T. Sionneau), nicolas.tribovillard@univ-lille1.fr (N. Tribovillard), aloys.bory@univ-lille1.fr (A. Bory), bflower@marine.usf.edu (B.P. Flower), armelle.riboulleau@univ-lille1.fr (A. Riboulleau), p.martinez@epoc.u-bordeaux1.fr (P. Martinez), i.billy@epoc.u-bordeaux1.fr (I. Billy).

Keywords: Mississippi River - Pigmy Basin – Holocene - atmospheric configuration - clay mineralogy – geochemistry

Abstract

Changes in terrigenous-transfer patterns from North America toward the Gulf of Mexico via the Mississippi River during the Holocene were investigated using mineralogical and geochemical records from the northern Gulf of Mexico (Pigmy Basin). Clay mineralogy (smectite/illite+chlorite) and geochemical signatures (K and Ti intensities) indicate fluctuations in the detrital sedimentation during the Holocene in the Pigmy Basin. They likely reflect alternations between at least two dominant terrigenous sources: the smectite-rich NW Mississippi watershed, and the illite- and chlorite-rich Great Lakes province and NE Mississippi watershed. These recurring and rapid modifications of erosional processes over this period suggest changes in the hydrological regime via rainfall patterns. Such a

modification during the Holocene is likely linked with the rapid atmospheric reorganization following the final collapse of the Laurentide Ice Sheet. Indeed, mineralogical and geochemical proxies indicate east-to-west migrations of the main detrital source (from the Great Lakes and northeastern province toward the northwestern province) associated with Mississippi River megaflood episodes. These modifications of the main detrital sources likely record migrations of the precipitation belt, which are constrained by atmospheric configuration (Jet Stream, Bermuda High and Intertropical Convergence Zone position) and subtropical oceanic hydrological properties (meridional extension of the Atlantic Warm Pool). In the frame of previously published rainfall patterns over the Caribbean and North America, our results highlight some marked modifications of moisture transfer throughout the Holocene. These changes are interpreted as resulting from two atmospheric configurations that have driven alternately the precipitation distribution over North America for the last 10 ka with an apparent cyclicity of ~2.5 ka. The coherent common cyclicity between the Gulf of Mexico detrital parameters and Greenland atmospheric proxies over the Holocene suggests that the initial external forcing was rapidly transferred latitudinally through atmospheric processes.

1. Introduction

The Gulf of Mexico (GOM) is ideally located for studying the relationships between high-latitude climate variability and subtropical hydrology. The hydrological properties of the GOM, that further impact the Gulf Stream, result from the complex interactions between the inflow of warm tropical waters originating from the Caribbean Sea through the Loop Current, and from evaporation–precipitation budget and North American Rivers freshwater supply (Fig. 1a). The warm waters of the GOM, Caribbean Sea, and western tropical North Atlantic constituting the so-called Atlantic Warm Pool (AWP) represent the primary moisture source for North America (Wang and Enfield, 2001). Moisture meridian transfer is constrained by different atmospheric configurations, resulting from the respective position of the Jet Stream, the Bermuda High pressure cell and the Intertropical Convergence Zone (ITCZ) (Fig. 1a; Forman et al., 1995; Liu and Fearn, 2000; Knox, 2003; Harrison et al., 2003). The position of the main precipitation belt is therefore likely influenced by both low- and high-latitude forcing. All these oceanic and atmospheric characteristics are seasonally modulated. In the western tropical Atlantic Ocean, the AWP reaches its northern position during boreal summer when the ITCZ is located in its northern position, whereas these tropical waters are restricted to the southeastern GOM during boreal winter when the ITCZ is situated southward (Wang

and Enfield, 2001; Poore et al., 2004; Nürnberg et al., 2008; Ziegler et al., 2008).

The hydrological characteristics of the GOM are thus also largely impacted by freshwater outflow from the Mississippi River. The Mississippi and Missouri River watersheds and their tributaries collect runoff from almost half the USA and carry suspended detrital particles that are characteristic of the drained areas. Major Mississippi outflows may modify the sea-surface salinity and impact to some extent the thermohaline circulation via the Gulf Stream (Aharon, 2003; Flower et al., 2004). The Holocene climate is characterized by modifications of both atmospheric and oceanic configurations following the final collapse of the Laurentide Ice Sheet (LIS) evolution (Shuman et al., 2002). For instance, the Mississippi River was affected during the late Holocene by megaflood episodes resulting from recurrent modifications of both moisture transfer and precipitation regimes. During these episodes, massive erosion of the alluvial plains promoted the remobilization of fine-grained sediments and their transport toward the GOM via the Mississippi (e.g., Knox, 2000, 2003). These episodes were likely controlled by the atmospheric configuration, and may have resulted in changing the main provenance of the detrital supply and thus its mineralogical characteristics.

Recent studies (Sionneau et al., 2008; Montero-Serrano et al., 2009; Sionneau et al., 2010) suggest that variations of the clay mineral assemblage deposited in the northern GOM mainly reflect changes in the respective contributions of four main mineralogical provinces on land (Fig. 1b): (1) the northwestern Mississippi and Missouri rivers watershed is characterized by high smectite content (SN50%, Ib30%, Kb20%, Cb14%), (2) the northeastern province mainly delivering illite and chlorite (Sb20%, IN30%, Kb25%, CN12%), (3) the kaolinite-rich southeastern part of the United States (Sb30%, Ib20%, KN30%, Cb28%), and (4) the Brazos River and southwestern Mississippi River watersheds is dominated by illite and kaolinite (Sb40%, IN30%, KN20%, Cb8%). More details on the clay mineral distributions in and around Mississippi River watershed are discussed by Sionneau et al. (2008). The letters S, I, C and K denote smectite, illite, chlorite and kaolinite, respectively. The mineralogical and geochemical characteristics of the detrital fraction of the sediment can thus be used to trace the modifications of the main detrital source associated with major flooding episodes and to constrain the main factors triggering such catastrophic events.

In this article we present a mineralogical and geochemical record of Holocene climate variability for the last 10 ka from core MD02-2553 (27°11.01"N, 91°25.00"W, water depth 2259 m) recovered in the Pigmy Basin. This basin, situated on the Louisiana continental slope around 250 km southwest of the present-day Mississippi Delta, is suitably located to record both the terrigenous input from the North American continent and the tropical oceanic

104 influences via the Loop Current (Fig. 1a). The basin is approximately 20 km-long, 7 km-wide,
105 and trends northeast to southwest (Fig. 1b). Thus, using proxies of terrigenous supply in the
106 Pigmy Basin during the Holocene, the main objectives are: (1) to determine changes in the
107 North American sedimentary provenance throughout the Holocene, (2) to document the main
108 changes in rainfall distribution over North America, and (3) to constrain the links between
109 modifications of both high-latitude and subtropical domains, in order to infer possible
110 synoptic scenarios or configurations of the atmosphere–ocean–continent interactions during
111 the Holocene, and to further constrain the Holocene variations in summer moisture transfers
112 across North America.
113
114 **2. Materials and methods**
115 *2.1. Samples and chronology*
116 The samples were taken from the 10.3 m long core MD02-2553 (Calypso Square)
117 collected on the center of the Pigmy Basin during the 2002 PAGE (Paleoceanography of the
118 Atlantic and Geochemistry) cruise of the research vessel Marion Dufresne, as part of the
119 International Marine Past Global Changes Study (IMAGES) program (Fig. 1b). The sediment
120 is mainly composed of massive or faintly laminated silty to clayey mud (Fig. 1c). Black
121 shading related to accumulation of organic material is recurrent throughout the core. The
122 uppermost 155 cm of the core is composed of sandy to silty clay with foraminifers and
123 coccoliths, whereas the lower part contains clays with foraminifers that become scarce below
124 400 cm. One distinct upward grading, foraminifer-rich, sandy layers interpreted as small
125 turbidites occurring in the core at 298–300 cm depth has been removed from the record, as it
126 corresponds to local sedimentological processes rather than fluvial discharge.
127 The chronology for the upper 359 cm of core MD02-2553 is based on sixteen
128 accelerator mass spectrometry (AMS) 14C radiocarbon dates from mixed planktic
129 foraminifers published by Poore et al. (in press) (Table 1, Fig. 1c). All ages were converted
130 into calendar years with the CALIB software (Stuiver and Reimer, 1993, version 5.0.2;
131 http://calib. qub.ac.uk/calib), using the calibration curve Marine04 (Hughen et al., 2004). All
132 AMS14C ages were corrected using a constant reservoir age of 400 yr ($\Delta R=0$) because it
133 provides consistency with both modern values (Bard, 1988) and with previous
134 paleoceanographic studies from the GOM (e.g., Flower et al., 2004; Meckler et al, 2008;
135 Nürnberg et al., 2008; Montero-Serrano et al., 2009). Calibrated ages were plotted against
136 core depth (Fig. 2), and a least squares regression ($r2=0.996$) indicates a linear sedimentation
137 rate of 35.9 cm/ka (within the errors of the calibrated dates; 1 ka=1000 cal yr BP) and a core-

top age of 0 yr BP.

2.2. Analytical methods

The Holocene section of the core MD02-2553 (the upper 359 cm) was studied at high resolution (average sample resolution of ~47 yr) for clay mineralogy and grain size. Inorganic geochemistry was studied for some major elements (K and Ti) at 1 cm resolution (average sample resolution of ~28 yr) using the XRF core scanner. Complementarily, trace and rare earth element (REE) concentrations were determined at lower resolutions, with average sample resolution of 555 yr.

2.2.1. Clay mineral analysis

Clay mineral associations were studied using X-ray diffraction following the protocol of Bout-Roumazeilles et al. (1999). The analyses were run from 2.49°θ to 32.49°2θ on a Philips PW 1749 diffractometer (copper anode; 40 kV; 25 mA intensity and 1°2θ/minute speed). Three X-ray diagrams were performed, after air-dried sample, ethylene glycol vapour saturation for 12 h and heating at 490 °C during 2 h. Semi-quantitative estimation of clay mineral abundances (smectite, illite, chlorite and kaolinite), based on peak areas, was performed using the Macintosh MacDiff® 4.2.5 software (Petschick, 2000). The error on the reproducibility of measurements is estimated to be 5% for each clay mineral, as checked by analysis of replicate samples.

2.2.2. Grain-size distribution

Grain-size analyses were carried out on the carbonate-free fraction of the sediment, in order to focus on the detrital fraction, using a Malvern Mastersizer 2000 laser diffractometer. Sample preparation and optical settings for the Mastersizer 2000 followed the method described by Montero-Serrano et al. (2009). The main grain-size parameter reported here is the mode (μm, most frequent grain size). The precision was ~4%, expressed as the coefficient of variation of replicate determinations.

2.2.3. Elemental geochemistry

K and Ti abundances were obtained on the U-channels of the core using the Avaatech XRF core scanner at the Université Bordeaux 1 (EPOC, UMR-CNRS 5805). The U-channels used were designed and developed at the Paleomagnetism and Environmental Magnetism laboratory of the LSCE (Gif-sur-Yvette, France). The U-channels surface was cleaned and

covered with Ultralene® X-ray transmission foil to avoid desiccation of the sediment and contamination of the measurement unit. To obtain statistically significant data we used a 30 s count time, a 10 kV X-ray voltage and a current of 400 mA. Acquired XRF spectra were processed with the WinAxil and WinBatch software packages. The resulting data are expressed as element intensities in counts per second (cps). Precisions were better than 2%, as checked by international standards powder samples. For further technical details on the XRF scanning technique see Richter et al. (2006).

In addition to XRF core scanner, trace and rare earth element (REE) concentrations were determined by inductively coupled plasma optical emission spectrometry (ICP-OES) and inductively coupled plasma mass spectrometry (ICP-MS), at Activation Laboratories Ltd. (Ancaster, Canada). Samples were mixed with a flux of lithium induction furnace. Molten sample was immediately poured into a solution of 5% nitric acid (HNO3) containing an internal standard, and mixed continuously until completely dissolved. The analytical accuracy and precision were found to be better than 5–10% for trace element and 5% for REE, as checked by international standards and analysis of replicate samples.

Trace-metal (TM) concentrations are expressed in terms of enrichment factors (EFTM) where the Al-normalized metal concentration is compared to the average shale values of Wedepohl (1971, 1991): EF_{TM}=TM/Al_{sample}:TM/$Al_{average\ shale}$. $EF_{T>}$N1 suggests enrichment relative to average shale but authigenic enrichments can be considered when EF_{TM} exceeds 5 (Tribovillard et al., 2006). NASC values by Gromet et al. (1984) are used for normalization of the REE.

In this study, K and Ti intensities are used as proxies of the detrital sediment sources, complementary to clay mineral proxies. In addition, the REE abundance patterns provide fingerprints associated with detrital fraction of the sediment which in turn represents the bulk composition (e.g., Montero-Serrano et al., 2009).

2.3. Spectral analyses

We performed time series analysis in order to evidence any cyclicity in the Pigmy basin clay mineral variations and to investigate their correlation with high-latitude climatic records, using the software package AnalySeries 2.0.4 (Paillard et al., 1996; http:// www.lsce.ipsl.fr/logiciels/index.php). We used two different spectral analysis methods a non-parametric Multi-Taper method, which provides high spectral resolution even for short time series (Thompson, 1982) and the high confidence Blackman–Tukey method (Blackman and Tukey, 1958) in order to improve accuracy and to prevent any bias due to methodological

206 artefact. All time series were evenly resampled with a 0.045-ka interval and linear trends were
207 removed prior to spectral analysis. The sample interval results in an average time resolution
208 of 0.045 ka. Thus the lowest theoretical period (Nyquist period) that could be resolved is
209 always below 0.167 ka (two times maximum sampling period). Spectral analyses were
210 calculated for the b5.88 ka (1/0.17 ka) high-pass filtered data, according to the studied
211 window 9.99 ka. The multi-taper method (MTM; Ghil et al., 2002) was performed using two
212 tapers and a bandwidth resolution of 0.3 ka. The Blackman–Tukey cross-spectral analysis
213 (Paillard et al., 1996) was performed using a Bartlett-type window, high resolution (50% of
214 the series length) with a resulting 0.30 ka−1 bandwidth. Results of the spectral analysis are
215 presented as spectral density. Each frequency band is reported taking as center the observed
216 maximum spectral density for specific band. The mean Blackman–Tukey coherency and
217 phase were calculated by cross-spectral analysis between the clay mineral distribution
218 [S/(I+C)] in the Pigmy Basin and GISP2 sea-salt Na record (O'Brien et al., 1995; Mayewski et
219 al., 2004). Coherency is considered significant (at the 95% level) if larger than 0.67.
220 Averaged coherency is calculated on the 0.30 ka bandwidth centered on S/(I+C) maximum
221 power spectrum. Phases are reported only for the more significant bands (highest spectral
222 density and significant coherency). Phases in radians were converted to kiloyears (one
223 period=360°=2Pi radian) for each of the frequency bands.
224 All analytical data presented are available through the World Data Center-A for
225 Paleoclimatology.[1]
226
227 **3. Results**
228 *3.1. Clay mineralogy and sediment grain size*
229 The clay mineral fraction is composed of 56–84% smectite, 7–20% illite, 3–14%
230 chlorite and 3–13% kaolinite (Fig. 3). In general, smectite distribution is inversely correlated
231 to illite and chlorite. The clay mineral composition displays some characteristic oscillations
232 between smectite-rich intervals (for example between 2.9 and 1.6 ka) and illite+ chlorite-rich
233 intervals (for example between 3.8 and 2.9 ka).
234 All samples are characterized by a unimodal grain-size distribution. The sediments are
235 mainly composed of cohesive-silt (3.5 μm <mode> 5.1 μm). The grain-size mode (μm) shows

[1] 1 Supporting data are available electronically at Wold Data Center (WDC Paleo online archive; e-mail: paleo@mail.ngdc.noaa.gov, URL: ftp://ftp.ncdc.noaa.gov/pub/data/paleo/contributions_by_author/montero-serrano2010/montero-serrano2010.xls.

a steady and rather constant distribution throughout the Holocene (Fig. 4a). The important point is that the rather smooth distribution in the grain-size mode suggests that the mineralogical and elemental variations within the studied core are not due to the sorting of the sediment (e.g., Fig. 4b–d).

3.2. Geochemical composition of the sediment

The XRF core scanner provides a record of the main geochemical variations characterizing the sediments from the Pigmy Basin. K and Ti records display similar trends, (Fig. 4c,d consistent with the observed clay mineral oscillations, i.e., K and Ti intensities are maximum over the illite+chlorite-rich intervals (Fig. 4b–d)). Fig. 4 also shows the opposed relationship between K and Ti and the smectite proportion within the sediment. Elemental intensities are thus interpreted to reflect changes in the clay mineral assemblage of the terrigenous fraction. Trace-metal enrichment factors do not show any significant variations (0.5 to 2.2) (Fig. 5a). NASC-normalized REE patterns do not show any striking features (Fig. 5b), except for a general slight enrichment in light REE (LREE: La–Nd) over heavy REE (HREE: Tb–Lu).

4. Interpretation and discussion

4.1. Main characteristics of Holocene sedimentary records in the Pigmy Basin

The calcareous biogenic fraction in the Pigmy Basin sediments is relatively low (CaCO3b25%; not shown) indicating that the Holocene sedimentation is mostly terrigenous, with a relatively limited, autochthonous biogenic contribution. In addition, detrital carbonate contributions in the Pigmy sediments are negligible, as evidenced by the scanning electron microscopy (SEM) analysis of silt-size particles from the same core (Flocks and Swarzenski, 2007). Furthermore, trace-metal enrichment factors suggest that the authigenic phases in the Pigmy Basin are negligible (Fig. 5a). The absence of any significant REE fractionation when normalized to NASC in Pigmy Basin sediments, as observed in other basins from the GOM (Flocks and Swarzenski, 2007), indicates a smoothed detrital source (Fig. 5b). The similarity of REE distributions in Pigmy Basin sediments when compared with Mississippi River suspended loads (Goldstein and Jacobsen, 1988; Elderfield et al., 1990) indicates the dominant influence of the Mississippi River (Fig. 5b). Our results thus suggest that the Pigmy Basin is representative of the sedimentation in the offshore part of the GOM in that it mainly collects land-derived particles delivered by the Mississippi River which receives main discharges from the Missouri (NW)+Ohio (NE) rivers system (e.g., Sionneau et al., 2008) and

drains almost half of the conterminous USA (Fig. 1b). In other words, the Pigmy Basin is an appropriate recorder of the land-to-sea transfer, from North America to the GOM.

Mineralogical and geochemical data both suggest that Holocene detrital sedimentation mainly results from the contributions of two different sources. The first source is characterized by its high smectite content whereas the second contributor is enriched in illite and chlorite with high K and Ti intensities (Figs. 3 and 4). According to recently published clay mineral distribution maps (Sionneau et al., 2008), the first end-member corresponds to the northwestern Mississippi and Missouri rivers watershed province and the second, one is likely the northeastern Great Lakes province.

During the early Holocene, the Mississippi River discharge capacity was significantly reduced compared with the last deglaciation (Fig. 2), as evidenced in the Pigmy Basin record by a decrease of the sedimentation rate from about 397–200 during the Meltwater Spike (Montero-Serrano et al., 2009) to 25–36 cm/ka during the Younger Dryas and Holocene. This decrease is due to a drastic decrease in the glacial erosional processes linked to the decay of the Laurentide Ice Sheet or LIS (Montero-Serrano et al., 2009). The modifications of the LIS extent (e.g., Fig. 8a) played a major role in climate change in the Northern Hemisphere between 10 and 5 ka, resulting in the rapid warming of the Northern Hemisphere interrupted by the cold 8.2 ka event (Mayewski et al., 2004). Consequently, the observed variations in the respective contributions of these two dominant sources (smectite vs. illite+chlorite) during the early Holocene may be related to the LIS extent changes.

Any major modification of the dominant terrigenous sources that occurred during the middle to late Holocene cannot be driven by the LIS that was considerably reduced by this time. Significant modifications are more likely related to modifications of the continental drainage patterns on the Mississippi River system in response to migrations of the main precipitation belt over North America (Knox, 2000, 2003). The mineralogical and geochemical record of core MD02- 2553 from the Pigmy Basin will thus be here interpreted in relation with the Holocene climatic variability.

4.2. The variability of Mississippi River runoff during the Holocene

Successive intervals enriched in smectite [S/(I+C)>4] characterize Holocene Pigmy Basin records (Fig. 6c). These intervals at 10–8.9, 8–6.2, 5–3.8, 2.9–1.6, 0.8–0.3 ka coincide with large Mississippi floods (Fig. 6a) described in the central part of North America (Knox, 2000, 2003). Note that K intensities show a parallel trend when compared with illite and an opposite trend when compared with smectite, reflecting its affinity for K-bearing illite in

304 sediments from Pigmy Basin (Fig. 6b). These observations suggest that the mineralogical
305 signature is indeed influenced by erosional processes in the NW Mississippi watersheds.
306 These Holocene flood episodes, occurring as the ice-sheet had almost entirely
307 vanished, likely resulted from heavy rainfall periods over the central part of North America
308 (Knox, 2003). Additionally, the smectite-rich interval observed in the Holocene in the Pigmy
309 Basin was already described in the Orca Basin (Sionneau, 2008) and interpreted as a period of
310 severe megafloods (Brown et al., 1999). The correlations between continental and marine
311 records indicate that these megaflood events represent regional-scale changes in the
312 hydrologic cycle over North America.
313 We hypothesize that the variability of the Mississippi River regime during the
314 Holocene (e.g., flood episodes) evidenced by both mineralogical and geochemical records
315 reflects primarily variations in the migration of the precipitation belt over the North American
316 continent. According to this scenario, these variations have been controlled by changes in
317 atmospheric circulation patterns and the associated modifications of the meridian moisture
318 transfer from the GOM to the North American continent. This moisture transfer and more
319 generally the hydrological variability directly depend on the evaporation (E)–precipitation (P)
320 balance over the GOM (Knox, 2000; Harrison et al., 2003) where increased evaporation leads
321 to enhanced precipitation over the North American continent (e.g., Flannery et al., 2008). As
322 the E–P balance is linked to insolation, and sensitive to solar irradiance variability (Perry and
323 Hsu, 2000), we also hypothesize that changes in solar variability may ultimately affect rainfall
324 patterns over North America through ocean–atmosphere interactions. We will further test this
325 hypothesis by comparing our records with previously published climate-related records from
326 the Caribbean, GOM and North America.
327
328 *4.3. Precipitation distribution and atmospheric configuration during the Holocene*
329 The interaction of three main air masses controls the general climatic patterns over the
330 North American continent: the warm and moist GOM air mass, the dry and mild Pacific air
331 mass, and the dry, cold Arctic air mass (Knox, 2000). The location of the boundary between
332 these air masses in North America, and therefore of the main position of the precipitation
333 front, is controlled by the respective position and extension of the Jet Stream, and of the
334 Bermuda High pressure and Thermal Low pressure cells (Forman et al., 1995; Liu and Fearn,
335 2000; Knox, 2003). In the northwestern Mississippi river watershed, where the smectite-rich
336 intervals are associated with paleo-flooding episodes (Fig. 6), present-day average annual
337 precipitation ranges between about 498 and 568 mm with about 70% of the annual amount

falling during the warm season from April to September (boreal summer; http://www.rssweather.com/climate/).

Here we attempt to use clay mineral record from the Pigmy Basin to retrace the summer migrations of the precipitation belt over the central part of North America during the Holocene. The contributions of smectite vs. illite+chlorite [S/(I+C) ratio] from the Pigmy Basin are used to document the continental-scale shift of the precipitation belt over the central part of North America. Additionally, we use previously published palynological, isotopic and geochemical data from both continental and marine series (Hodell et al., 1991; Haug et al., 2001; Willard et al., 2005; Kennedy et al., 2006; Denniston et al., 2007; Nordt et al., 2008; Mueller et al., 2009) in order to constrain the two proposed configurations of the Holocene variations in summer ocean–continent moisture transfer (Forman et al., 1995; Knox, 2000, 2003; Liu and Fearn, 2000).

The signal of Holocene climatic conditions over North America is reconstructed using different proxies. A shift toward positive values in the Δ%C4 records of buried soils from the North American Great Plains (Nordt et al., 2008) and in the δ13C records of stalagmites from the Devil's Icebox Cave (Denniston et al., 2007), is interpreted to indicate increased abundances of C4 grasses (Δ%C4) and hence warming and drying conditions; conversely negative values suggest wetter conditions. Increased aridity is inferred from reconstructed increases in percent of Quercus pollen from the Chesapeake Bay, (Willard et al., 2005).

4.3.1. Configuration 1

The mineralogical and geochemical signatures of the smectite-rich intervals (10–8.9, 8–6.2, 5–3.8, 2.9–1.6, 0.8–0.3 ka; Figs. 6 and 7e) indicate that the major flood events were derived primarily from northwestern Mississippi and Missouri rivers watersheds. These results suggest that the precipitation belt was located over the northwestern province and that the main moisture transfer reached the central part of North America during these periods. Negative Δ%C4 excursions from the North American Great Plains (Fig. 7d) also suggest an enhanced moisture flux from the GOM toward the central part of North America, whereas the strong increase in the Quercus pollen content from the Chesapeake Bay (Fig. 7b) in the northeastern region of the North America, indicates the development of drought conditions along the eastern coast of North America. Furthermore, several northeastern USA lakes also experienced low level during these intervals implying a widespread drought (e.g., Newby et al., 2000; Shuman et al., 2002). According to configuration 1, the moisture distribution

evidenced during these intervals implies that the Jet Stream and the Bermuda High were located to their northernmost and southwestern most positions, respectively, while the low pressure was displaced eastward (configuration 1, Fig. 9c) in agreement with configurations proposed by Forman et al. (1995), Liu and Fearn (2000) and Knox (2000, 2003). At present, this synoptic pattern promotes transfer of moist air from the GOM and nearby tropical waters toward the central part of North America (Knox, 2000, 2003).

4.3.2. Configuration 2

The intervals 8.9–8, 6.2–5, 3.8–2.9 and 1.6–0.8 ka are characterized by low S/(I+C) ratio (Fig. 7e) indicating low precipitation on the smectite-rich northwestern province. This suggests an eastward transfer of the main moisture pattern, which is consistent with the relative increase in illite and chlorite. Positive Δ%C4 and δ13C excursions from the North American Great Plains (Fig. 7d) and the Devil's Icebox Cave, central Missouri (Fig. 7c) also suggest dry conditions over the central part of North America. On the contrary, the strong decrease in the Quercus pollen content from the Chesapeake Bay (Fig. 7b) suggests enhanced moisture abundance in the mid- Atlantic region (Willard et al., 2005). All these observations enable us to propose a second configuration (configuration 2) of the main moisture transfer over the successive intervals depleted in smectite (Fig. 9d). Investigations on the regional hydrologic responses to large-scale atmospheric circulation patterns during the Holocene (e.g., Forman et al., 1995; Knox, 2000, 2003; Liu and Fearn, 2000; Harrison et al., 2003; Goman and Leigh, 2004) suggest that the Jet Stream and the Bermuda High were located to the south and northeast respectively constraining the inflow of moisture along the eastern coast of North America and a reduced flux toward the central part of North America. The reconstructed Jet Stream pattern shown in Fig. 9d with a main meridional component and a noticeable zonal component would likely lead to warm and dry summer conditions in the central part of North America, while increased precipitation and flooding occurred in the eastern area (Knox, 2000, 2003).

4.3.3. Configuration modulation

The two proposed configurations are mainly based on GOM and North American records, i.e. related to the position of the Jet Stream and high- and low-pressure cells. In order to improve these scenarios, we attempt to take into account the variations of the ITCZ and AWP that may modulate moisture transfer throughout the Holocene. The ITCZ migration and the temporal dynamics of the AWP can be monitored using paleoclimate records from the

circum-Caribbean region and northern GOM (Figs. 1a and 8a–c,f). The relative abundance of the warm water species G. sacculifer and the seasurface temperature ($SST_{Mg/Ca}$) values in the GOM are related to the inflow of Caribbean water into the GOM. Maximum transport of Caribbean surface waters into the GOM, and therefore enhanced moisture transfer toward the central part of North America (Lovvorn et al., 2001), are associated with both a more pronounced AWP and a northward migration of the average position of the ITCZ.

In this context, the increase abundance of the warm water species G. sacculifer together with high $SST_{Mg/Ca}$ values from the GOM (Fig. 8c,f) and more negative δ18O values from the Miragoane Lake suggest that during the early Holocene, the AWP reaches its maximum size and intensity, in phase with a northward most position of the ITCZ, compared with the late Holocene (Fig. 8c,f). This position led to enhanced precipitation in the circum-Caribbean region and decreased the transport of precipitable water (E>P) toward the North American continent (Fig. 9c–d). However, during the late Holocene, a less established AWP, in combination with a southward position of the ITCZ (based on lower levels of G. sacculifer and low $SST_{Mg/Ca}$ in the GOM, and more positive #18O values from the Miragoane Lake; Fig. 8b–c) likely promoted drought in the Caribbean region (Figs. 8a and 9e–f), increasing the availability of precipitable water vapour (E>P) transported toward the North American continent (Wang et al., 2008). Thus during the past 3 ka, configuration 1b (Fig. 9e) is thought to be responsible for the more important flood events and catastrophic hurricanes that affected the central part of North America (e.g., Knox, 2000, 2003; Liu and Fearn, 2000).

4.4. Clay mineralogy variations during the Glacial–Holocene transition

The Holocene clay mineralogy variability in the Pigmy Basin sediments is similar in range with the Glacial–Holocene transition variability. There is a slight difference during the main meltwater discharge episode during the deglaciation (the Meltwater Spike; 15.2– 13 ka) when the S/(I+C) ratio reached 9 whereas the ratio remains below 8 during the Younger Dryas and Holocene which is characterized by the lowest S/(I+C) ratio (Fig. 9a). The results highlight variations in the contribution and nature of terrigenous particles eroded and transported by the Mississippi River towards the GOM interpreted as changing origin in response to climate influences through the last 15 ka. Under this frame, the modifications of provenance were predominantly linked to dynamics and timing of deglacial meltwater discharge originating from the south margin of the LIS (such as the Meltwater Spike; Fig. 9b) during the glacial periods (e.g., Licciardi et al., 1999; Flower et al., 2004;Montero-Serrano et al., 2009; Sionneau et al., 2010) whereas successive migrations of the precipitation belt over

North America (Fig. 9c–f) resulting from the changing moisture transfer patterns became a dominant process during ice-free intervals, during the Holocene (e.g., Brown et al., 1999; Knox, 2000, 2003; Liu and Fearn, 2000).

Complementarily, we observed that the middle to late Holocene trend of the K (and Ti) intensities is similar to the trend in the abundance of G. sacculifer (Poore et al., in press) in the same core (Fig. 8e–f). However, during the early Holocene these two records show a little correspondence. We interpret this lack of correlation as resulting from the impact of the LIS on continental climatic variability over the early Holocene (Fig. 7a). The ice-sheet probably filtered and smoothed the influence of the ITCZ and AWP on the main moisture flux trajectories and migrations of the precipitation belt over North America. As a result, continental processes probably responded slowly to the initial solar forcing because the LIS highly impacted regional temperatures at least until 6 ka (e.g., Lovvorn et al., 2001; Mayewski et al., 2004; Nordt et al., 2008). After the collapse of the LIS (~6 ka), rapid atmospheric reorganization (Shuman et al., 2002) triggered rapid hydrological changes over the central part of North America during the middle to late Holocene. The K (and Ti) variations are synchronous with changes in the abundance of G. sacculifer (Fig. 8e–f) during this time, suggesting that the influence of southern climate variations (such as ITCZ and AWP) seems to become dominant over hydrological and erosional processes in the Mississippi River watershed. These interpretations are in agreement with previous studies from the GOM and the Caribbean region (e.g., Poore et al., 2003; Richey et al., 2007, 2009; Wang et al., 2008).

To summarize, the Pigmy Basin sedimentary record suggests that the variations of the Mississippi River supply are mainly controlled by the glacigenic processes resulting from the decaying of the southern margin of LIS during the deglaciation and early Holocene, whereas atmosphere–ocean interactions become the main forcing during middle to late Holocene once the LIS had collapsed.

4.5. Forcing of the atmosphere–ocean–continent oscillations—teleconnections

The observed link between climatic variability (wet vs. Dry periods), atmospheric configurations and clay mineral record are further evaluated using spectral analysis (Fig. 10). The clay mineral assemblage variations, previously attributed to changes in the precipitation belt over North America, are similar to oscillations evidenced in the Holocene glaciochemical records from the GISP2 ice core (O'Brien et al., 1995; Mayewski et al., 2004). Clay mineral (notably, illite+chlorite rich intervals) exhibits variations very similar with maximum sea-salt

sodium (ssNa) concentrations (Fig. 10a–b). Note that smectite-rich intervals in the Pigmy Basin are inversely correlated to high GISP2 ssNa concentrations. The ssNa in the GISP2 ice core is believed to be an indicator of storminess and sea spray in the atmosphere of the high-latitude region. Thus, the variability of the Mississippi River runoff appears to be correlated with changes in high-latitude atmospheric circulation. Cross-spectral analysis, using the Multi-Taper (Ghil et al., 2002) and Blackman– Tukey methods (Paillard et al., 1996) between the clay mineral distribution [S/(I+C) ratio] in the Pigmy Basin and GISP2 ssNa record displayed the same periodicity centered around 2.5 ka (Fig. 10c). The S/(I+C) and GISP2 ssNa signals are coherent at 95% confidence level in the 2.5 ka frequency band with an average phase of 1.05±0.09 ka. The results confirm that precipitations and erosional processes in the NE Mississippi River watershed have been in phase with periods of intense atmospheric circulation in Greenland. Consequently, these results suggest a link between large-scale atmospheric circulation changes in the high-latitude North Atlantic and the hydrological and erosional changes in the North American continent.

The 2.5 ka periodicity also characterized ice rafted debris (IRD) occurrences in North Atlantic marine sediments (Debret et al., 2007, 2009), the $\delta^{18}O$ record in GISP2 ice core (Alley et al., 1997), and solar irradiance cycles (Stuiver et al., 1995). The correspondence between our mineralogical data and North Atlantic paleoclimate records may be due to modulation of atmospheric dynamics by solar forcing (Debret et al., 2009).

5. Summary and conclusions

Mineralogical and geochemical records of Holocene sediments from the Pigmy Basin (GOM) reveal fluctuations of the Mississippi River discharge. They reflect alternations between two dominant terrigenous sources (smectite vs. illite+chlorite), which are interpreted as successive migrations of the main precipitation belt over North America. Holocene sedimentation in the northern GOM is characterized by recurrent occurrences of smectite-rich intervals associated with documented flooding episodes of the Mississippi River. Their mineralogical signatures point out to specific terrigenous supply from the NW Mississippi river watershed, suggesting enhanced precipitations and moisture influx from the GOM toward central North America. Instead, repetitive enrichments in illite and chlorite and high K intensities suggest successive eastward migrations of main precipitation belts, consistent with documented evidence of increased aridity over central North America and development of more humid conditions along the Atlantic margin.

These data provide additional information to those previously published on the North

American continent, Caribbean region and GOM. Their confrontation allows documenting the variations of the main moisture flux trajectories over North America and of the associated precipitation belt during the Holocene. Our mineralogical records evidence two main atmosphere–ocean configurations that successively control moisture transfer and precipitation distribution over North America throughout the Holocene:

(1) The northern position of the Jet Stream and southwest migration of the Bermuda High promoted the influx of moisture over the central part of North America which may have triggered flooding of the Mississippi River about 10–8.9, 8–6.2, 5–3.8, 2.9–1.6 and 0.8–0.3 ka ago. On the opposite, the northeastern provinces experienced dry conditions.

(2) The southern position of the Jet Stream associated with a northeastward displacement of the Bermuda High constrained the main moisture flux along the Atlantic margin about 8.9–8, 6.2–5, 3.8–2.9 and 1.6–0.8 ka ago.

Oscillations of these two configurations promoted the repetitive occurrence of drought/flooding over the northwestern Mississippi River through the Holocene. These two configurations correlate with both continental and oceanic records in North America and the Caribbean, and take into account the mean position of the ITCZ and AWP that modified moisture balance (E–P) over the GOM and ultimately affected the hydrologic variability over the North American continent. The previously discussed aspects suggest thus that during the Holocene the main moisture flux trajectories and migrations of the precipitation belt over North America were mainly constrained by the respective positions of the Jet Stream and Bermuda High modulated by displacements of both ITCZ and AWP.

Spectral analysis shows a coherent common cyclicity of 2.5 ka between mineral proxies from the Pigmy Basin and the Greenland sea-salt sodium record suggesting a tight chronological connection between atmospheric circulation changes in the high-latitude North Atlantic and the hydrological and erosional changes in the North American continent. This synchronism underlines the major role played by the atmosphere compared with the ocean in the moisture transfers over North America, because processes involving the ocean would have induced a time lag between the respective records of the high latitudes and GOM settings.

Acknowledgements

We thank Yvon Balut, the Institut Paul-Emile Victor (IPEV), the officers and crew of the R/V Marion Dufresne and the IMAGES program for core collection. This study was financially supported by: (1) the Laboratoire Géosystèmes (FRE 3298 CNRS) of the Université Lille 1 (France), and (2) the Programme Alban, the European Union Programme of

541 High Level Scholarships for Latin America, scholarship E06D100913VE. We thank the
542 technical staff of the Géosystèmes lab: Léa-Marie Emaille, Laurence Debeauvais, Deny
543 Malengros, Philippe Recourt and Déborah Ponleve. V.B.R. thanks Laurent Labeyrie for
544 initiating the IMAGES-PAGE cruise. Thanks also to Richard Poore, Debra Willard, Lee
545 Nordt, Dirk Nürnberg, Paul Mayewski and David Hodell for providing data. This article
546 benefited from the reviews and suggestions of Anna Nele Meckler. Lastly, thanks to the two
547 anonymous reviewers for improving this article through careful review, and to Sierd
548 Cloetingh for his editorial work.
549
550 **References**
551 Aharon, P., 2003. Meltwater flooding events in the Gulf of Mexico revisited: implications for
552 rapid climate changes during the last deglaciation. Paleoceanography 18 (4), PA1079.
553 doi:10.1029/2002PA000840.
554 Alley, R.B., Mayewski, P.A., Sowers, T., Stuiver, M., Taylor, K.C., Clark, P.U., 1997.
555 Holocene climatic instability: a prominent, widespread event 8200 yr ago. Geology 25, 483–
556 486.
557 Bard, E., 1988. Correction of accelerator mass spectrometry 14C ages measured in planktonic
558 foraminifera: paleoceanographic implications. Paleoceanography 3 (6), 635–645.
559 Blackman, R.B., Tukey, J.W., 1958. The measurement of power spectra from the point of
560 view of communication engineering. Dover Publications. 190 pp.
561 Bout-Roumazeilles, V., Cortijo, E., Labeyrie, L., Debrabant, P., 1999. Clay-mineral evidence
562 of nepheloid layer contribution to the Heinrich layers in the Northwest Atlantic.
563 Palaeogeography, Palaeoclimatology, Palaeoceanography 146, 211–228.
564 Brown, P., Kennett, J.P., Ingram, B.L., 1999. Marine evidence for episodic Holocene
565 megafloods in North America and the northern Gulf of Mexico. Paleoceanography 14 (4),
566 498–510.
567 Debret, M., Bout-Roumazeilles, V., Grousset, F.E., Desmet, M., McManus, J.F., Massei, M.,
568 Sebag, D., Petit, J.R., Copard, Y., Trenteseaux, A., 2007. The origin of the 1500-year climate
569 cycles in Holocene North-Atlantic records. Climate of the Past 3, 569–575.
570 Debret, M., Sebag, D., Crosta, X., Massei, N., Petit, J.-R., Chapron, E., Bout-Roumazeilles,
571 V., 2009. Evidence from wavelet analysis for a mid-Holocene transition in global climate
572 forcing. Quaternary Science Reviews 28, 2675–2688.
573 Denniston, R.F., DuPree, M., Dorale, J.A., Asmerom, Y., Polyak, V.J., Carpenter, S.J., 2007.
574 Episodes of late Holocene aridity recorded by stalagmites from Devil's Icebox Cave, central

575 Missouri, USA. Quaternary Research 68, 45–52.
576 Dyke, A.S., 2004. An outline of North American deglaciation with emphasis on central and
577 northern Canada. In: Ehlers, J., Gibbard, P.L. (Eds.), Quaternary Glaciations – Extent and
578 Chronology, Part II. Elsevier B.V, Amsterdam, pp. 373–424.
579 Elderfield, H., Upstill-Goddard, R., Sholkovitz, E.R., 1990. The rare earth elements in rivers,
580 estuaries and coastal seas and their significance to the composition of ocean water.
581 Geochimica et Cosmochimica Acta 54, 971–991.
582 Flannery, J.A., Richey, J.N., Meckler, A.N., Hollander, D.J., 2008. A 1400 Year Multi-Proxy
583 Record of Hydrologic Variability in the Gulf of Mexico: Exploring Ocean–Continent
584 Linkages During the Late Holocene. Poster Presentation, 2008 ASLO Ocean Sciences
585 Meeting. online at: http://www.marine.usf.edu/PPBlaboratory/pages_students/ flannery
586 (Revised 2009-04-01).
587 Flocks, J., Swarzenski, P., 2007. Sediment collection from Orca and Pigmy basins, Gulf of
588 Mexico, and analyses for texture and trace-metal concentrations, July 2002, PAGE 127
589 Campaign. In: Winters, W.J., Lorenson, T.D., Paull, C.K. (Eds.), Initial Report of the
590 IMAGES VIII/PAGE 127 Gas Hydrate and Paleoclimate Cruise on the RV Marion Dufresne
591 in the Gulf of Mexico, 2–18 July 2002: U.S. Geological Survey Open-File Report 2004-1358,
592 one DVD. online at http://pubs.usgs.gov/of/2004/1358/.
593 Flower, B.P., Hastings, D.W., Hill, H.W., Quinn, T.M., 2004. Phasing of deglacial warming
594 and laurentide ice sheet meltwater in the Gulf of Mexico. Geology 32, 597–600.
595 Forman, S.L., Oglesby, R., Markgraf, V., Stafford, T., 1995. Paleoclimatic significance of late
596 Quaternary eolian deposition on the Piedmont and High Plains, central United States. Global
597 and Planetary Change 11, 35–55.
598 Ghil, M., Allen, M.R., Dettinger, M.D., Ide, K., Kondrashov, D., Mann, M.E., Robertson,
599 A.W., Saunders, A., Tian, Y., Varadi, F., Yiou, P., 2002. Advanced spectral methods for
600 climatic time series. Reviews of Geophysics 40, 1003. doi:10.1029/2000RG000092.
601 Goldstein, S.J., Jacobsen, S.B., 1988. Rare earth elements in river waters. Earth and Planetary
602 Science Letters 89, 35–47.
603 Goman, M., Leigh, D.S., 2004. Wet early to middle Holocene conditions on the upper coastal
604 plain of North Carolina. Quaternary Research 61, 256–264.
605 Gromet, L.P., Dymek, R.F., Haskin, L.A., Korotev, R.L., 1984. The North American shale
606 composite: its compilation, major and trace element characteristics. Geochimica et
607 Cosmochimica Acta 48, 2469–3482.
608 Harrison, S.P., Kutzbach, J.E., Liu, Z., Bartlein, P.J., Otto-Bliesner, B., Muhs, D., Prentice,

609 I.C., Thompson, R.S., 2003. Mid-Holocene climates of the Americas: a dynamical response to
610 changed seasonality. Climate Dynamics 20, 663–688.
611 Haug, G.H., Hughen, K.A., Sigman, D.M., Peterson, L.C., Roehl, U., 2001. Southward
612 migration of the intertropical convergence zone through the Holocene. Science 293, 1304–
613 1308.
614 Hodell, D.A., Curtis, J.H., Jones, G.A., Higuera-Gundy, A., Brenner, M., Binford, M.B.,
615 Dorsey, K.T., 1991. Reconstruction of the Caribbean climate change over the past 10, 500
616 years. Nature 352, 790–793.
617 Hughen, K.A., Baillie, M.G.L., Bard, E., Beck, J.W., Bertrand, C.J.H., Blackwell, P.G., Buck,
618 C.E., Burr, G.S., Cutler, K.B., Damon, P.E., Edwards, R.L., Fairbanks, R.G., Friedrich, M.,
619 Guilderson, T.P., Kromer, B., McCormac, G., Manning, S., Ramsey, C.B., Reimer, P.J.,
620 Reimer, R.W., Remmele, S., Southon, J.R., Stuiver, M., Talamo, S., Taylor, F.W., van der
621 Plicht, J.,Weyhenmeyer, C.E., 2004.Marine04marine radiocarbon age calibration, 0–26 cal
622 kyr BP. Radiocarbon 46, 1059–1086.
623 Kennedy, L.M., Horn, S.P., Orvis, K.H., 2006. A 4000-yr record of fire and forest history
624 from Valle de Bao, Cordillera Central, Dominican Republic. Palaeogeography,
625 Palaeoclimatology, Palaeoecology 231, 271–290.
626 Knox, J.C., 2000. Sensitivity of Modern and Holocene floods to climate change. Quaternary
627 Science Reviews 19, 439–457.
628 Knox, J.C., 2003. 2003. North American palaeofloods and future floods: responses to climate
629 change. In: Gregory, K.J., Benito, G. (Eds.), Palaeohydrology: Understanding Global Change.
630 J. Wiley and Sons, Chichester, pp. 143–164.
631 Licciardi, J.M., Teller, J.T., Clark, P.U., 1999. Freshwater routing by the Laurentide ice sheet
632 during the last deglaciation. In: Clark, P.U., et al. (Eds.), Mechanisms of Global Climate
633 Change at Millennial Time Scales, 112. American Geophysical Union Geophysical
634 Monograph, pp. 177–201.
635 Liu, K.B., Fearn, M., 2000. Reconstruction of prehistoric landfall frequencies of catastrophic
636 hurricanes in Northwestern Florida from lake sediment records. Quaternary Research 54,
637 238–245.
638 LoDico, J.M., Flower, B.P., Quinn, T.M., 2006. Subcentennial-scale climatic and hydrologic
639 variability in the Gulf of Mexico during the early Holocene. Paleoceanography 21, PA3015.
640 doi:10.1029/2005PA001243.
641 Lovvorn, M.B., Frison, G.C., Tieszen, L.L., 2001. Paleoclimate and Amerindians: evidence
642 from stable isotopes and atmospheric circulation. Proceedings of the National Academy of

643 Sciences 98, 2485–2490.
644 Mayewski, P.A., Rohling, E.E., Stager, J.C., Karlen, W., Maasch, K.A., Meeker, L.D.,
645 Meyerson, E.A., Gasse, F., vanKreveld, S., Holmgren, K., Lee-Thorp, J., Rosqvist, G., Rack,
646 F., Staubwasser, M., Schneider, R.R., Steig, E.J., 2004. Holocene climate variability.
647 Quaternary Research 62, 243–255.
648 Meckler, A.N., Schubert, C.J., Hochuli, P.A., Plessen, B., Birgel, D., Flower, B.P., Hinrichs,
649 K.-U., Haug, G.H., 2008. Glacial to Holocene terrigenous organic matter input to sediments
650 from Orca Basin, Gulf of Mexico—a combined optical and biomarker approach. Earth and
651 Planetary Science Letters 272, 251–263.
652 Montero-Serrano, J.C., Bout-Roumazeilles, V., Tribovillard, N., Sionneau, T., Riboulleau, A.,
653 Bory, A., Flower, B.P., 2009. Sedimentary evidence of deglacial megafloods in the northern
654 Gulf of Mexico (Pigmy Basin). Quaternary Science Reviews 28, 3333–3347.
655 Mueller, A.D., Islebe, G.A., Hillesheim, M.B., Grzesik, D.A., Anselmetti, F.S., Ariztegui, D.,
656 Brenner, M., Curtis, J.H., Hodell, D.A., Venz, K.A., 2009. Climate drying and associated
657 forest decline in the lowlands of northern Guatemala during the late Holocene. Quaternary
658 Research 71, 133–141.
659 Newby, P.E., Killoran, P., Waldorf, M.R., Shuman, B.N., Webb, R.S., Webb, T.I.I.I., 2000.
660 14, 000 years of sediment, vegetation, and water-level changes at the Makepeace Cedar
661 Swamp, southeastern Massachusetts. Quaternary Research 53, 352–368.
662 Nordt, L., Von Fischer, J., Tieszen, L., Tubbs, J., 2008. Coherent changes in relative C4 plant
663 productivity and climate during the late Quaternary in the North American Great Plains.
664 Quaternary Science Reviews 27, 1600–1611.
665 Nürnberg, D., Ziegler, M., Karas, C., Tiedemann, R., Schmidt, M.W., 2008. Interacting Loop
666 Current variability and Mississippi River discharge over the past 400 kyr. Earth and Planetary
667 Science Letters 272, 278–289.
668 O'Brien, S.R., Mayewski, P.A., Meeker, L.D., Meese, D.A., Twickler, M.S., Whitlow, S.I.,
669 1995. Complexity of Holocene climate as reconstructed from a Greenland ice core. Science
670 270, 1962–1964.
671 Paillard, D., Labeyrie, L., Yiou, P., 1996. Macintosh program performs time-series analysis.
672 AGU EOS Transactions 77, 379.
673 Perry, C.A., Hsu, K.J., 2000. Geophysical, archaeological, and historical evidence support a
674 solar-output model for climate change. Proceedings of the National Academy of Sciences 97,
675 12433–12438.
676 Petschick, R. 2000. MacDiff 4.2 Manual. MacDiff [Online]. Available from World Wide

Web: http://www.geologie.uni-frankfurt.de/Staff/Homepages/Petschick/RainerE. html (Revised 2009-04-01).

Poore, R.Z., Dowsett, H.J., Verardo, S., 2003. Millennial- to century-scale variability in Gulf of Mexico Holocene climate records. Paleoceanography 18, PA1048. doi:10.1029/2002PA000868.

Poore, R.Z., Quinn, T.M., Verardo, S., 2004. Century-scale movement of the Atlantic Intertropical Convergence Zone linked to solar variability. Geophysical Research Letters 31, L12214. doi:10.1029/2004GL019940.

Poore, R.Z., Verardo, S., Caplan, J., Pavich, K., Quinn, T., in press. Planktic foraminiferal relative abundance trends in the Gulf of Mexico Holocene sediments: records of climate variability. In Holmes, C., (Ed.), Gulf of Mexico, Its Origins, Waters, Biota, and Human Impacts. Univ Texas Press.

Richey, J.N., Poore, R.Z., Flower, B.P., Quinn, T.M., 2007. 1400 Yr multiproxy record of climate variability from the northern Gulf of Mexico. Geology 35, 423–426.

Richey, J.N., Poore, R.Z., Flower, B.P., Hollander, D.J., Quinn, T.M., 2009. Regionally coherent Little Ice Age cooling in the Atlantic Warm Pool. Geophysical Research Letters 36, L21703. doi:10.1029/2009GL040445.

Richter, T.O., van der Gaast, S., Koster, B., Vaasrs, A., Gieles, R., de Stigter, H.C., de Haas, H., van Weering, T.C.E., Rothwell, R.G., 2006. The Avaatech XRF Core Scanner: technical description and applications to NE Atlantic sediments. In: Rothwell, R.G. (Ed.), New Techniques in Sediment Core Analysis: Geological Society of London, Special Publication, 267, pp. 39–50.

Shuman, B., Bartlein, P., Logar, N., Newby, P., Webb III, T., 2002. Parallel climate and vegetation responses to the early-Holocene collapse of the Laurentide Ice Sheet. Quaternary Science Reviews 21, 1793–1805.

Shuman, B., Bartlein, P., Webb III, T., 2005. The magnitudes of millennial- and orbital scale climatic change in eastern North America during the Late Quaternary. Quaternary Science Reviews 24, 2194–2206.

Sionneau, T., 2008. Transferts Continent – Océan : Enregistrement du dernier cycle climatique par les sédiments terrigènes du Golfe du Mexique. PhD thesis, Université Lille 1. 377 p. online at http://tel.archives-ouvertes.fr/tel-00366377/fr/.

Sionneau, T., Bout-Roumazeilles, V., Biscaye, P.E., van Vliet-Lanoë, B., Bory, A., 2008. Clay-mineral distributions in and around Mississippi River watershed and Northern Gulf of Mexico: sources and transport patterns. Quaternary Science Reviews 27, 1740–1751.

Sionneau, T., Bout-Roumazeilles, V., Flower, B.P., Bory, A., Tribovillard, N., Kissel, C., Van Vliet-Lanoë, B., Montero-Serrano, J.C., 2010. Provenance of freshwater pulses in the Gulf of Mexico during the last deglaciation. Quaternary Research 74, 235–245.

Stuiver, M., Reimer, P.J., 1993. Extended 14C data-base and revised calib 3.0 14C age calibration program. Radiocarbon 35, 215–230.

Stuiver, M., Grootes, P.M., Braziunas, T.F., 1995. The GISP2 #18O climate record of the past 16, 500 years and the role of the sun, ocean, and volcanoes. Quaternary Research 44, 341–354.

Thompson, D.J., 1982. Spectrum estimation and harmonic analysis. Proceedings of the IEEE 70, 1055–1098.

Tribovillard, N., Algeo, T., Lyons, T.W., Riboulleau, A., 2006. Trace metals as paleoredox and paleoproductivity proxies: an update. Chemical Geology 232, 12–32.

Wang, C., Enfield, D.B., 2001. The tropical Western Hemisphere warm pool. Geophysical Research Letters 28, 1635–1638.

Wang, C., Lee, S.-K., Enfield, D.B., 2008. Climate response to anomalously large and small Atlantic warm pools during the summer. Journal of Climate 21, 2437–2450.

Wedepohl, K.H., 1971. Environmental influences on the chemical composition of shales and clays. In: Ahrens, L.H., Press, F., Runcorn, S.K., Urey, H.C. (Eds.), Physics and Chemistry of the Earth. Pergamon, Oxford, pp. 305–333.

Wedepohl, K.H., 1991. The composition of the upper Earth's crust and the natural cycles of selected metals. In: Merian, E. (Ed.), Metals and Their Compounds in the Environment. VCH-Verlagsgesellschaft, Weinheim, pp. 3–17.

Willard, D.A., Bernhardt, C.E., Korejwo, D.A., Meyers, S.R., 2005. Impact of millennial scale Holocene climate variability on eastern North American terrestrial ecosystems: pollen-based climatic reconstruction. Global and Planetary Change 47, 17–35.

Ziegler, M., Nürnberg, D., Karas, C., Tiedemann, R., Lourens, L.J., 2008. Persistent summer expansion of the Atlantic Warm Pool during glacial abrupt cold events. Nature Geoscience 1 (9), 601–605.

Figure captions

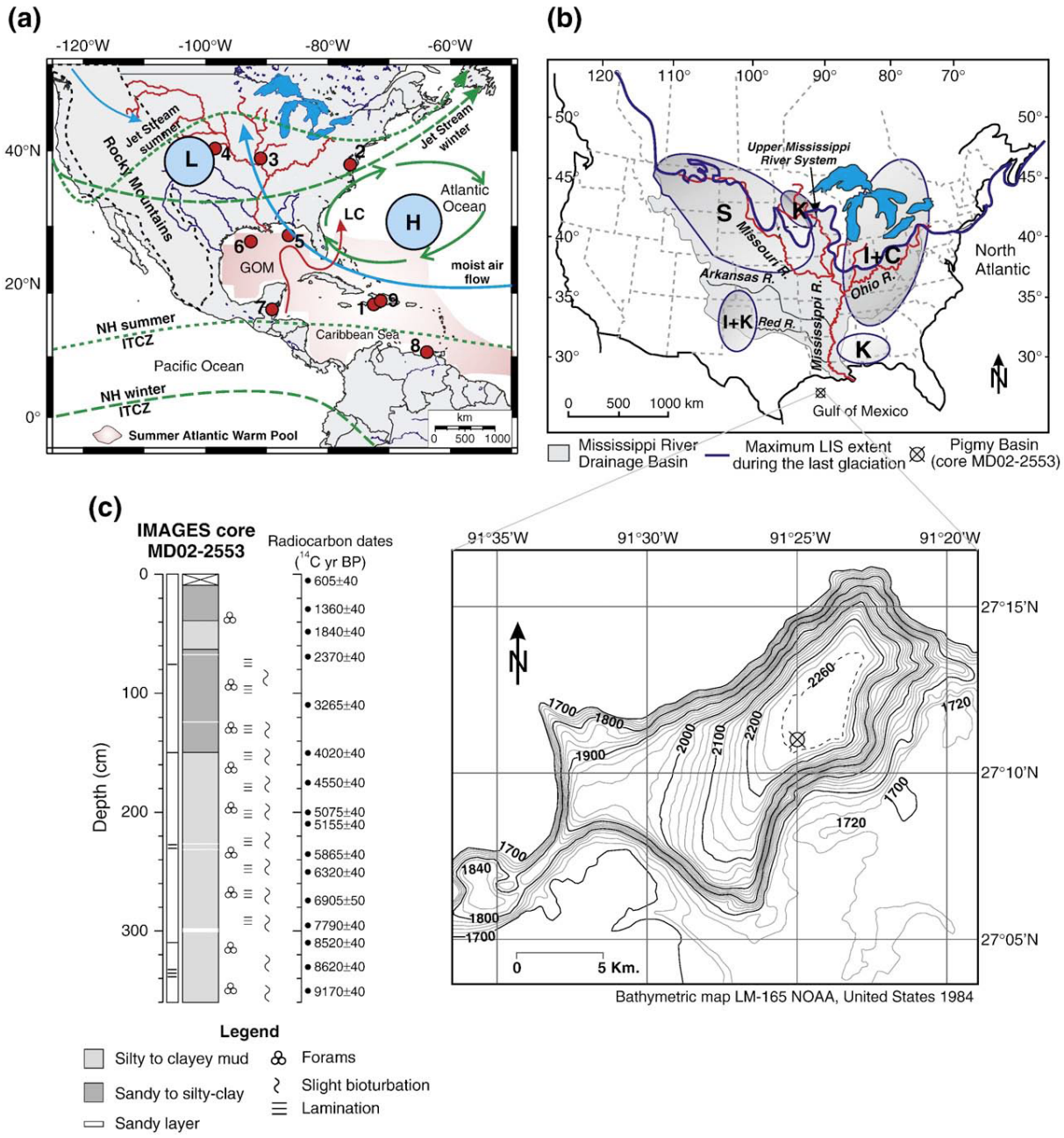

Fig. 1. (a) Map showing the location of selected localities discussed in this study, generalized position of the Intertropical Convergence Zone (ITCZ) for Northern Hemisphere (NH) winter and summer [adapted from Ziegler et al. (2008)], the summer position of the Atlantic Warm Pool [adapted from Wang and Enfield (2001)], the mean configuration of the Jet Stream during winter and summer regimes (adapted from Knox, 2000, 2003), and the mean summer position of the Bermuda High and the Thermal Low relative to North America [adapted from Forman et al. (1995) and Liu and Fearn (2000)]. (b) The Mississippi River watershed showing the main continental clay mineral provinces over the United States (Sionneau et al., 2008) and the Last Glacial Maximum extent of the Laurentide Ice Sheet (Dyke, 2004). The letters S, I, C

and K (standing for smectite, illite, chlorite and kaolinite, respectively) indicate areas where the bedrock/soils contain a clay mineral assemblage markedly dominated by one clay species. Note that the Mississippi River receives main discharges from the Missouri (NW)+Ohio (NE) rivers system, which drains almost half of the conterminous USA (e.g., Sionneau et al., 2008). GOM: Gulf of Mexico, LC: Loop Current. Numbers at each site are: (1) Lake Miragoane, Haiti; (2) Chesapeake Bay, northeastern of the North America; (3) Devil's Icebox Cave, central Missouri; (4) North American Great Plains, (5) DeSoto Canyon, northeastern GOM; (6) Pigmy and Oraca Basin, northern GOM; (7) Lake Petén Itzá, northern Guatemala; (8) Cariaco Basin, offshore northern Venezuela; (9) Cordillera Central, Dominican Republic. (c) Lithological log of core MD02-2553 between 0 and 360 cm showing the sedimentological characteristics and radiocarbon ages (Poore et al., in press).

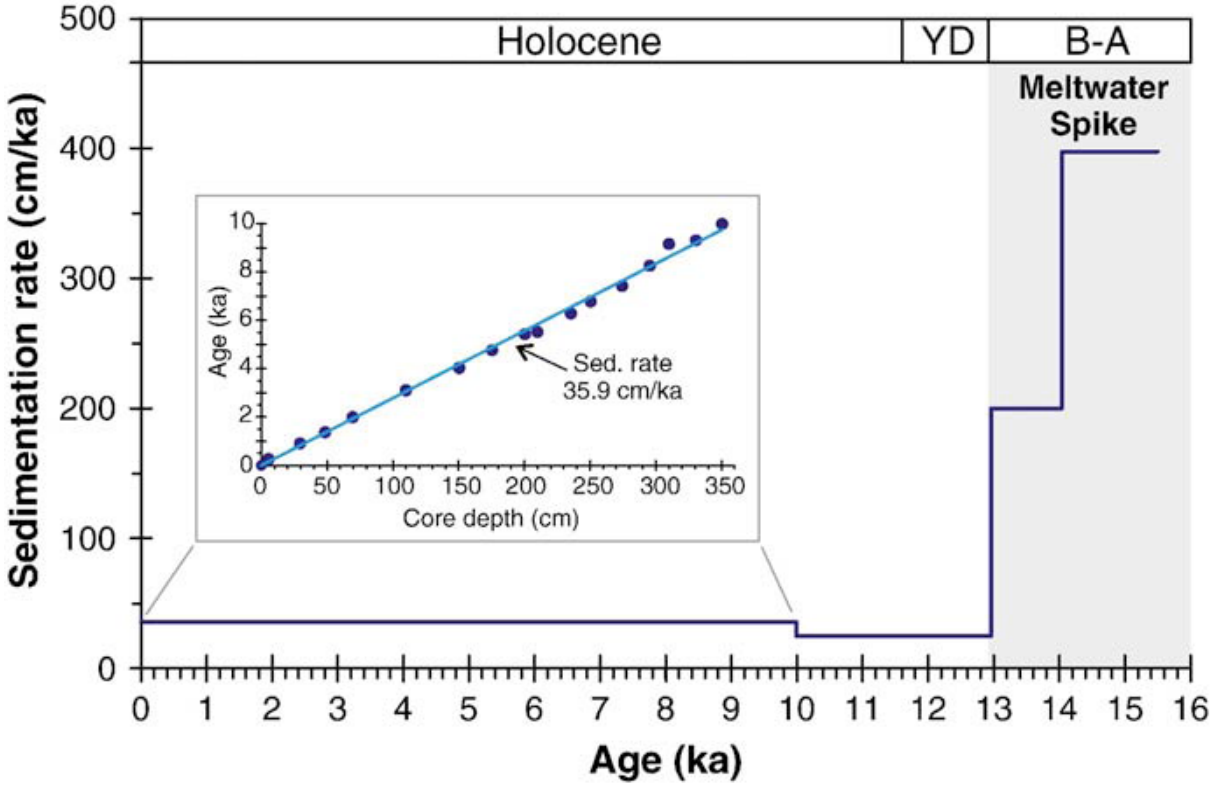

763

764 Fig. 2. Sedimentation rates of the Pigmy Basin (cores MD02-2553) in the GOM during the
765 Glacial–Holocene transition. The Younger Dryas (YD) from 12.9 to 11.6 ka and Bølling–
766 Allerød warming (B–A) from 15.4 to 12.9 ka are indicated. Data from 10 to 15.2 ka from
767 Montero-Serrano et al. (2009). Inset in left shows age model for core MD02-2553 based on
768 16 AMS 14C dates from mixed planktic foraminifers (Poore et al., in press), converted to
769 calendar ages (Table 1). Depth in centimeters was converted to calendar age by linear
770 interpolation (1 ka=1000 cal yr BP).

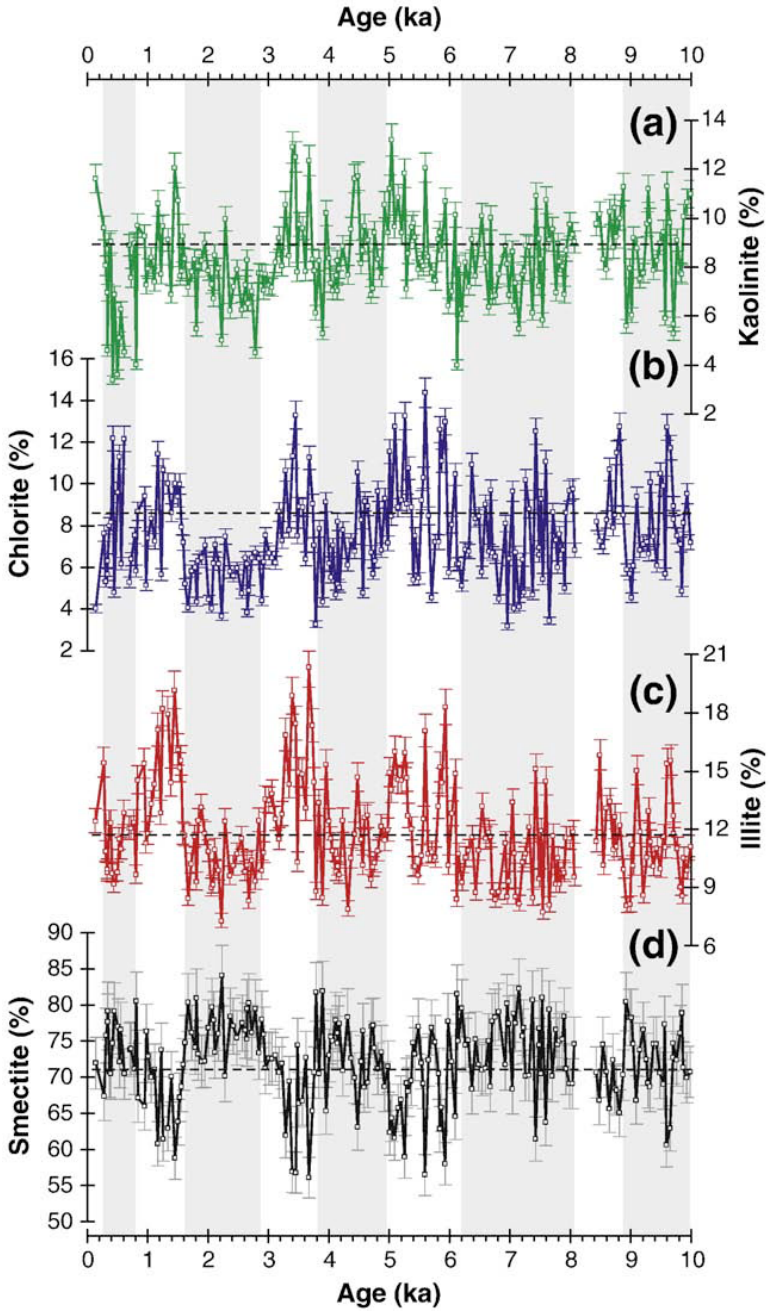

771

772 Fig. 3. Clay mineral assemblages from the Pigmy Basin (core MD02-2553). The horizontal
773 dotted lines indicate the mean concentrations for each clay mineral. The smectite-rich
774 intervals are indicated in gray bands. The semi-quantitative evaluation of each clay mineral
775 has an accuracy of ~5%.

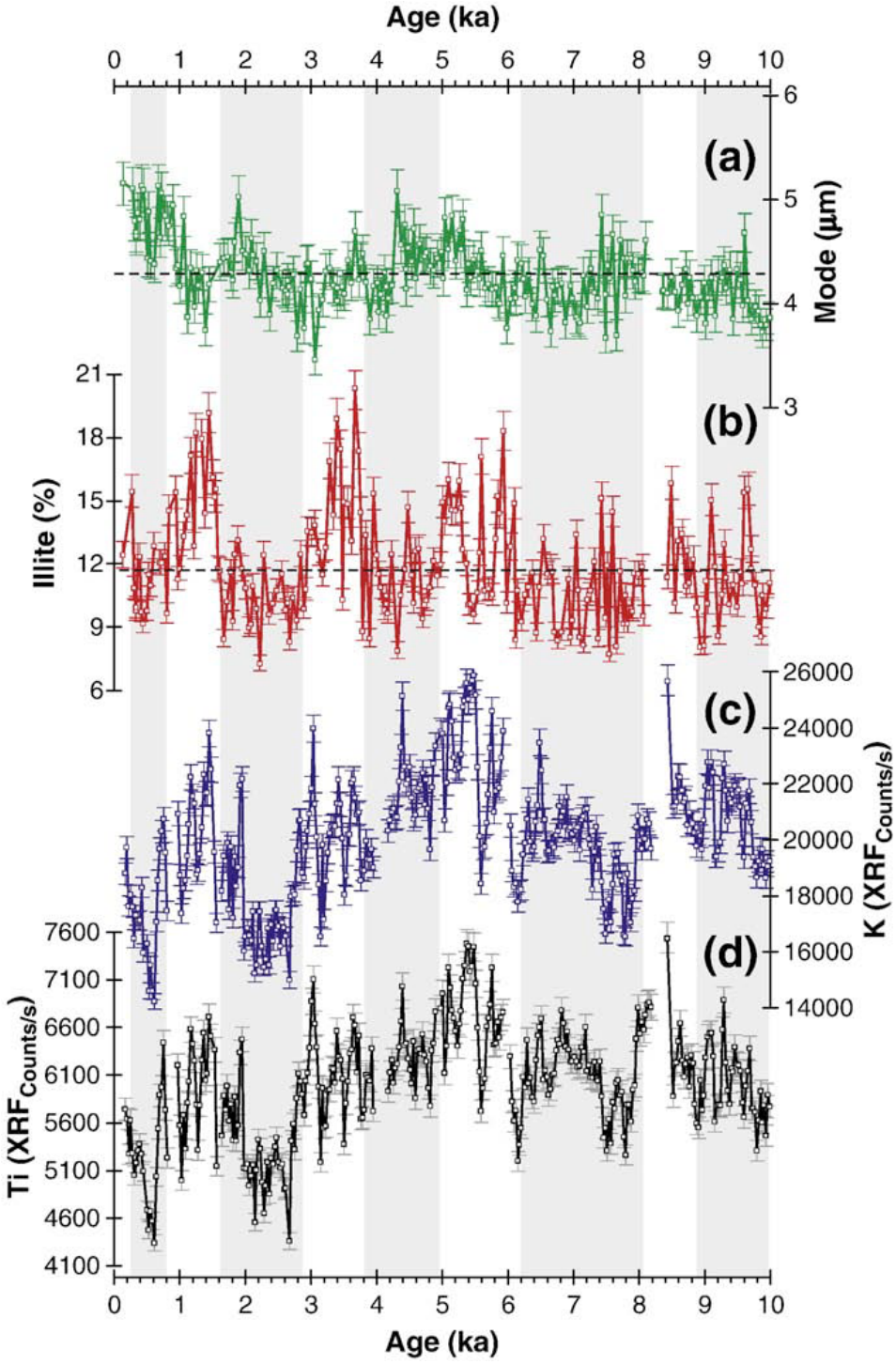

Fig. 4. Comparison of sedimentological and geochemical records from the Pigmy Basin (core MD02-2553). (a) Grain-size mode distributions (μm), (b) illite (%), and (c–d) K and Ti intensities in counts per second. The horizontal dotted lines indicate the mean concentrations for the grain-size mode and illite. Clay mineral, grain-size and XRF core scanner analyses have accuracy better than 5%, 4% and 2%, respectively. The smectite-rich intervals are indicated in gray bands.

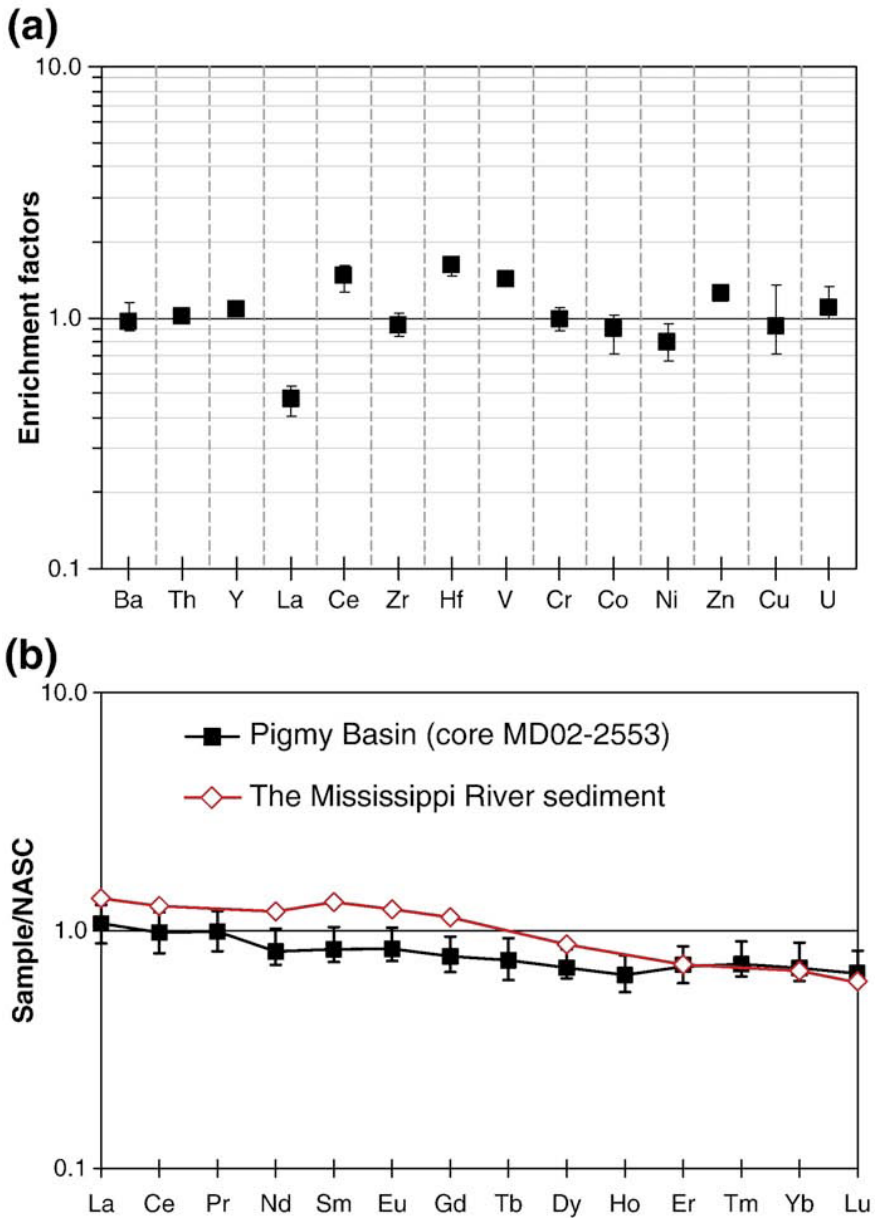

784

785 Fig. 5. (a) Comparisons of the enrichment factor of selected trace metals of core MD02- 2553
786 (Pigmy Basin). The extent line of the boxes corresponds to the range of values (min–max)
787 and the boxes to the average value. The horizontal line EF=1 indicates the value for which
788 there is no enrichment/depletion with regards to average shale composition. (b) Comparison
789 of REE patterns between the averages of the Pigmy Basin and Mississippi River sediments
790 (Goldstein and Jacobsen, 1988; Elderfield et al., 1990). NASC values by Gromet et al. (1984)
791 are used for normalization. The analytical accuracy and precision were found to be better than
792 5–10% for trace element and 5% for REE, as checked by international standards and analysis
793 of replicate samples.

794

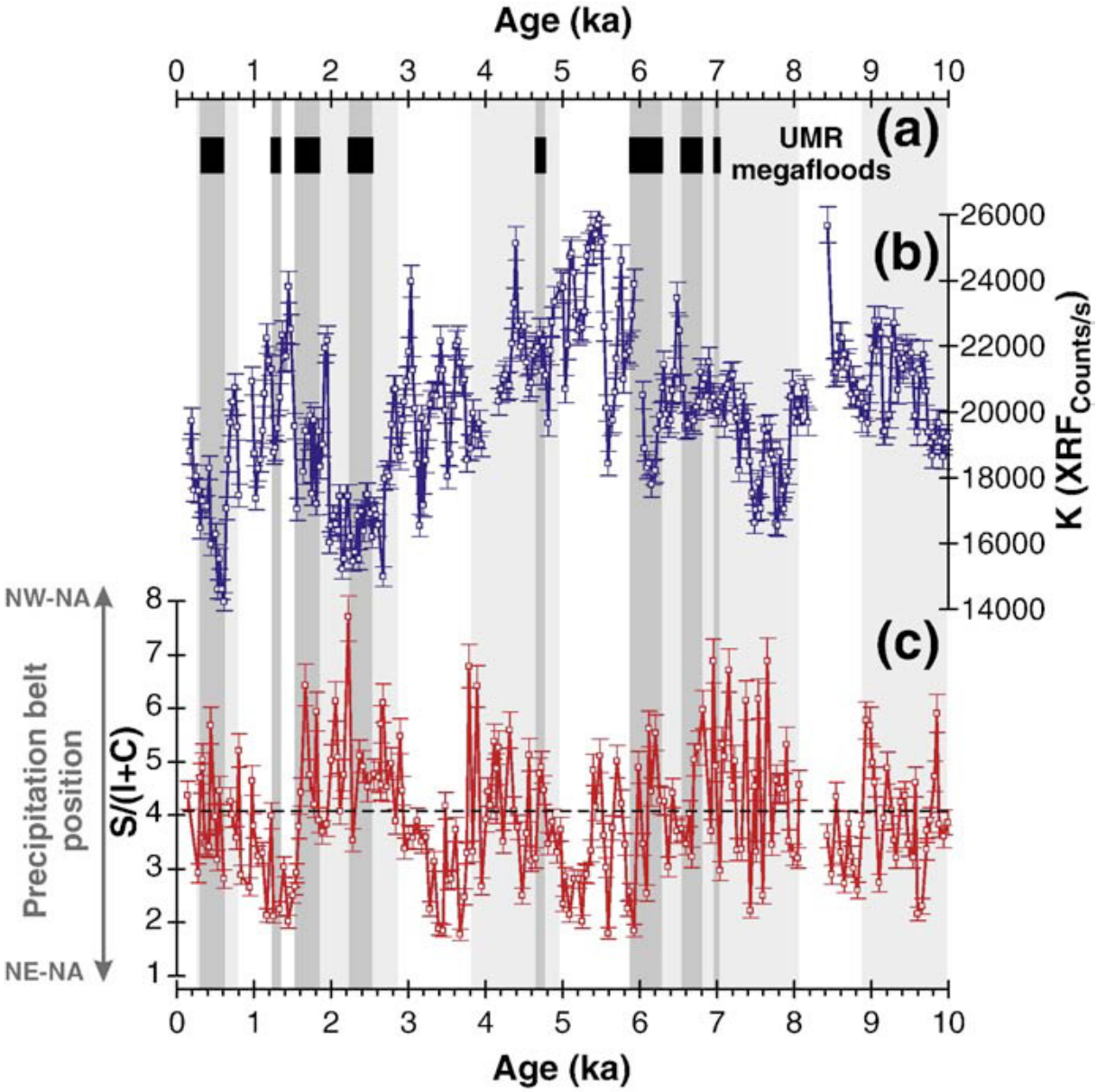

795

796 Fig. 6. Comparison of the mineralogical [S/(I+C) ratio] and geochemical records (K
797 intensities) of Holocene sediments from the Pigmy Basin (GOM) with the Upper Mississippi
798 River (UMR) channel megafloods episodes (Knox, 2003) from the central part of North
799 America (dark gray bands). Based on a simple error propagation, error on S/(I+C) ratio is
800 about 6%. XRF core scanner analyses have accuracy better than 4%. The smectite-rich
801 intervals are indicated in light gray bands.

802

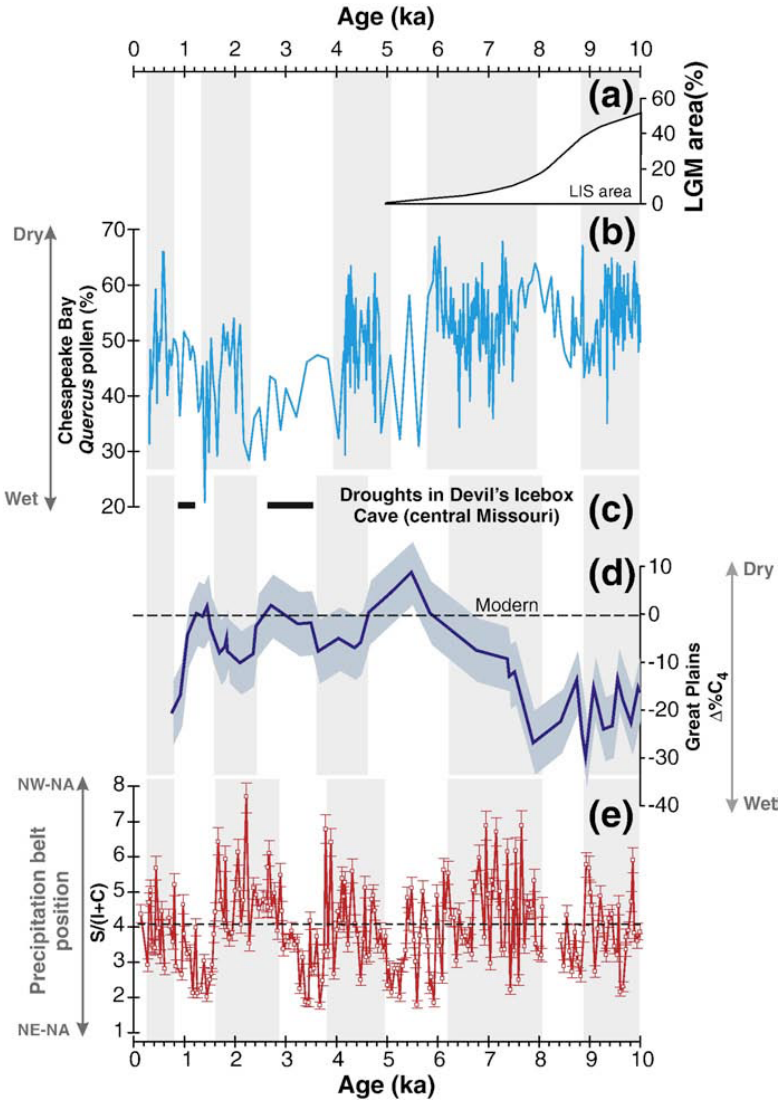

Fig. 7. Comparison of the mineralogical signature recorded in the Pigmy Basin (core MD02-2553) with the North American climate records: (a) the area of the Laurentide ice sheet (LIS) as a fraction of the area during the last glacial maximum (LGM), adapted from Shuman et al. (2005); (b) palynological records from Chesapeake Bay, northeastern USA (Willard et al., 2005); (c) episodes of late Holocene aridity (based in positive $\delta^{13}C$ excursions) recorded by stalagmites from Devil's Icebox Cave, central Missouri, USA (Denniston et al., 2007); (d) isotopic analysis of soil organic carbon (Δ%C4) in the North American Great Plains (Nordt et al., 2008). Δ%C4 is derived from the equation $\Delta\delta^{13}C_{C4}=\delta^{13}C_{C4\ buried\ soil}-\delta^{13}C_{C4\ modern\ latitudinal}$ (see Nordt et al., 2008 for procedural details). (e) Smectite/(Illite+Chlorite) ratio from the core MD02-2553. Based on a simple error propagation, error on S/(I+C) ratio is about 6%. The smectite-rich intervals are indicated in gray bands. The differences in timing and phasing of the smectite-rich intervals in the GOM sediments and continental climatic interpretationsmost likely reflect uncertainties in the individual chronologies.

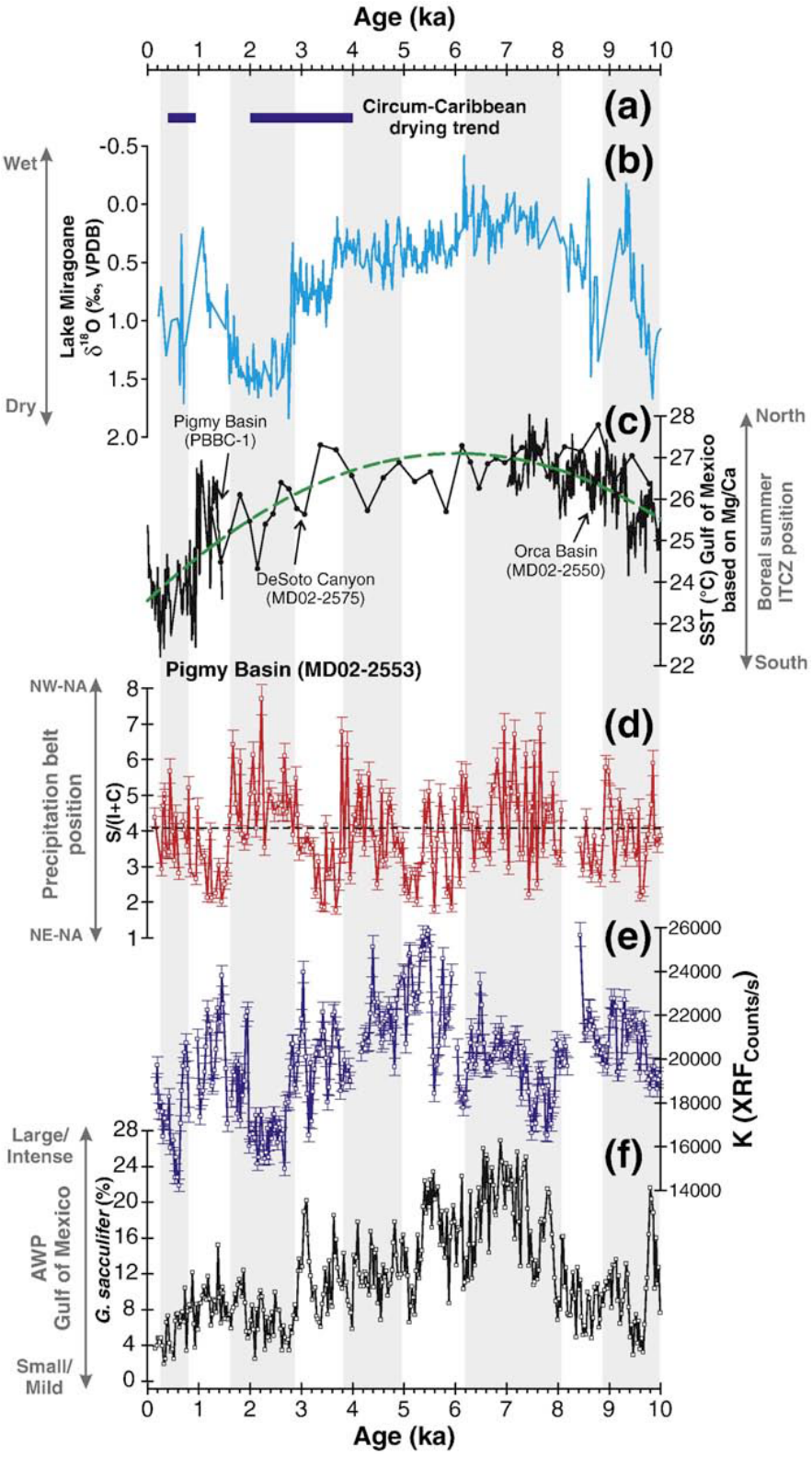

Fig. 8. Comparison of the multi-proxy record from the Pigmy Basin (core MD02-2553) with the Caribbean and GOM climate records: (a) previous interpretations of paleoclimate from the circum-Caribbean region. The Petén Itzá Lake (northern Guatemala; Mueller et al., 2009), Cordillera Central (Dominican Republic; Kennedy et al., 2006) and Cariaco Basin (offshore northern Venezuela; Haug et al., 2001); (b) oxygen isotope data from Lake Miragoane (Haiti;

Hodell et al., 1991). Original radiocarbon scale was converted to calendar year scale using CALIB 5.0.2 (Stuiver and Reimer, 1993); (c) composite records of sea-surface temperature (SST, °C) from GOM; core MD02-2550 from LoDico et al. (2006), core MD02-275 from Nürnberg et al. (2008) and core PBBC-1 from Richey et al. (2007); (d–e) mineralogical and geochemical proxies from the core MD02-2553; (f) relative abundance of the warm water species G. sacculifer in the northern GOM (core MD02-2553; Poore et al., in press). Variations in the G. sacculifer abundance in the GOM sediments are related to the influx of Caribbean surface waters into the GOM (expansion of the Atlantic Warm Pool) and the average position of the ITCZ (Poore et al., 2004). Based on a simple error propagation, error on S/(I+C) ratio is about 6%. XRF core scanner analyses have accuracy better than 4%. The smectite-rich intervals are indicated in gray bands.

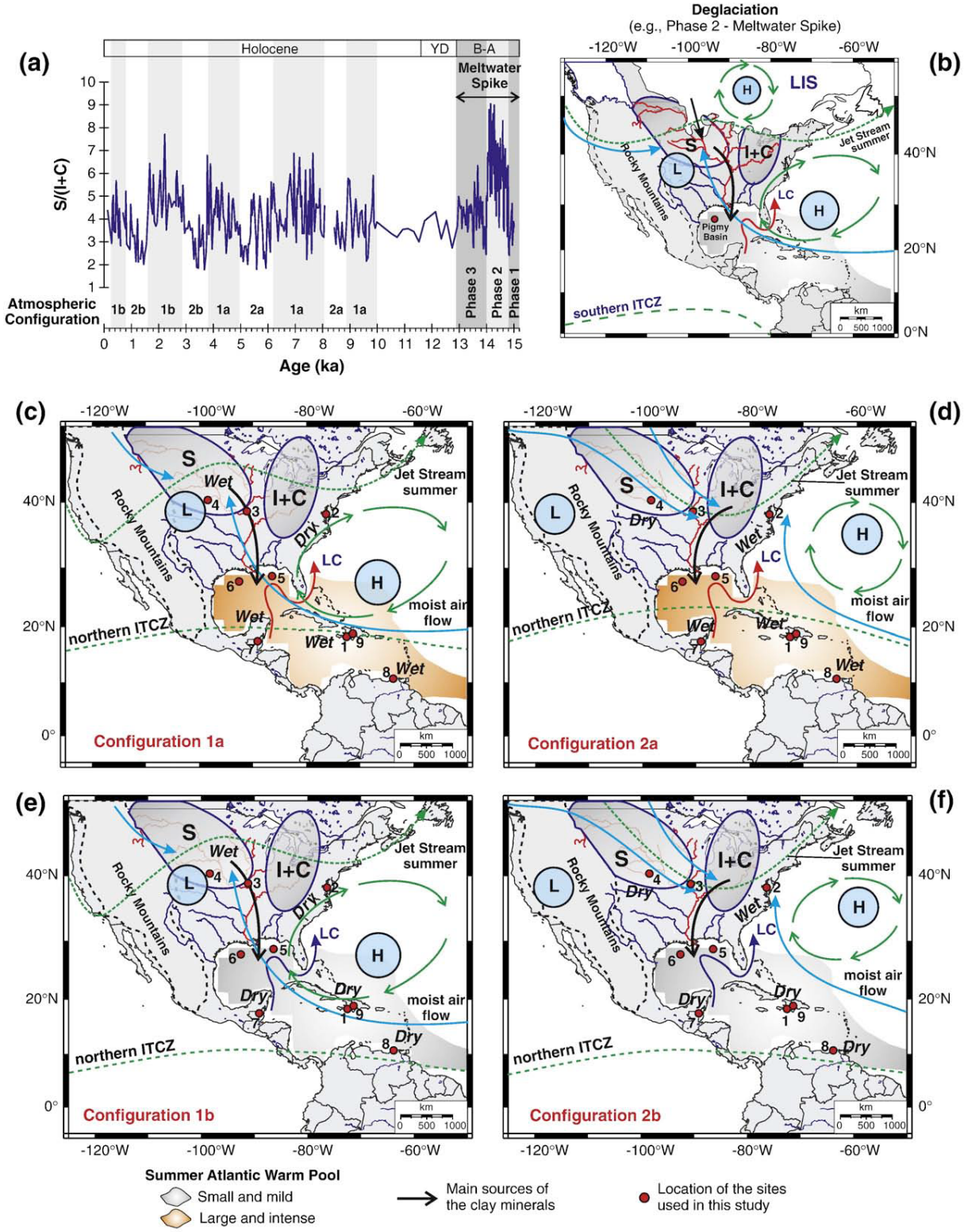

Fig. 9. (a) Clay mineral variations [S/(I+C) ratio] in the Pigmy Basin sediments during the Glacial–Holocene transition. The smectite-rich intervals are indicated in light gray bands. Dark gray bands denote intervals of the mixed provenance (smectite and illite+chlorite) of detrital particles during the deglaciation. Based on a simple error propagation, error on S/(I+C) ratio is about 6%. (b) Extent of the southern margin of Laurentide Ice Sheet during

841 the last deglaciation (~14.7 ka; Dyke, 2004), showing a dominant origin from NW North
842 America for detrital particles delivered to the GOM via the Mississippi River (Montero
843 Serrano et al., 2009). (c–f) Generalized reconstructions of regional atmospheric circulation
844 patterns during the Holocene summer in the middle-latitude North America and their
845 paleoclimatic implications. (c and e) Configurations during the predominant wet periods in
846 central North America (10–8.9, 8–6.2, 5–3.8, 2.9–1.6, 0.8–0.3 ka). (d and f) Configurations
847 during predominant dry periods in central North America (8.9–8, 6.2–5, 3.8–2.9 and 1.6–0.8
848 ka). The Jet Streams denote the approximate boundaries of air masses from the tropical,
849 paci!c and polar-source regions and locations of the areas with the main moisture transfers
850 over the North American continent (adapted from Knox, 2000, 2003). The mean summer
851 position of the Bermuda High and the Thermal Low relative to North America are modified
852 from Forman et al. (1995) and Liu and Fearn (2000). Note that the mean latitudinal shifts of
853 the Intertropical Convergence Zone (ITCZ) and meridional extension of the Atlantic Warm
854 Pool (AWP) through the Holocene are monitored using paleoclimate records from the circum-
855 Caribbean region and the northern GOM (Fig. 8a–c, f). Red and dark shade represents a more
856 and less established AWP. Numbers at each site are as in Fig. 1a.

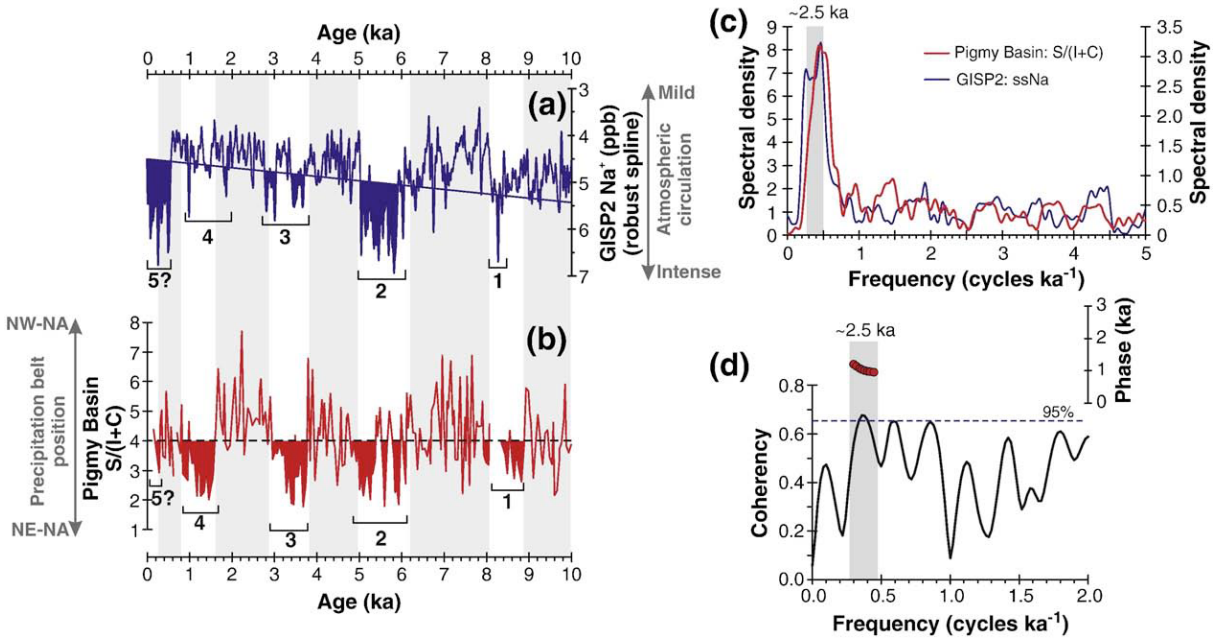

Fig. 10. (a) Holocene glaciochemical record from the GISP2 ice (O'Brien et al., 1995; Mayewski et al., 2004) compared with (b) clay mineral distribution [S/(I+C) ratio] from the Pigmy Basin. Numbers in (a) and (b) represent tentative correlations between the illite+chlorite-rich intervals of Pigmy sediments and intervals with high concentrations of GISP2 sea-salt sodium (ssNa; shaded values from O'Brien et al., 1995). NW-NA: northwestern North America, NE-NA: northeastern North America. Spectral analysis: (c) Multi-Taper spectral analysis of the S/(I+C) ratio and GISP2 sea-salt sodium (ssNa). (d) Cross-spectral analysis, based on the Blackman–Tukey method, between the S/(I+C) ratio and GISP2 ssNa record. Lower panel: coherency spectrum. Upper panel: phase. All periodicities signi!cant above 95% are labeled.

869 Table 1

870 Radiocarbon ages for core MD02-2553 (Poore et al., in press).

Core depth (cm)	Species	^{14}C AMS age (ka)	^{14}C Error (± yr)	Calibrated age (median, ka BP)	Calibarted error (± yr, 1 sigma)
0	Mixed planktic foraminifers	0		0	0
5.5		0.605	40	0.260	37
29.5		1.360	40	0.907	49
48.5		1.840	40	1.370	54
69.5		2.370	40	1.993	60
110.0		3.265	40	3.102	71
150.5		4.020	40	4.029	65
175.5		4.550	40	4.765	57
200.5		5.075	40	5.428	50
210.0		5.155	40	5.523	43
235.5		5.865	40	6.284	47
250.5		6.320	40	6.783	58
274.5		6.905	50	7.420	51
295.5		7.790	40	8.259	52
310.0		8.520	40	9.157	72
330.5		8.620	40	9.307	65
350.5		9.170	40	9.989	89

871